

The Impacts of Combined SAM and ENSO on Seasonal Antarctic Sea Ice Changes

JINFEI WANG,^a HAO LUO,^a LEJIANG YU,^b XUEWEI LI,^a PAUL R. HOLLAND,^c AND QINGHUA YANG^a

^a *School of Atmospheric Sciences, Sun Yat-sen University, and Southern Marine Science and Engineering Guangdong Laboratory (Zhuhai), Zhuhai, China*

^b *MNR Key Laboratory for Polar Science, Polar Research Institute of China, Shanghai, China*

^c *British Antarctic Survey, Cambridge, United Kingdom*

(Manuscript received 2 September 2022, in final form 17 December 2022)

ABSTRACT: Both the Southern Annular Mode (SAM) and El Niño–Southern Oscillation (ENSO) are critical factors contributing to Antarctic sea ice variability on interannual time scales. However, their joint effects on sea ice are complex and remain unclear for each austral season. In this study, satellite sea ice concentration (SIC) observations and atmospheric reanalysis data are utilized to assess the impacts of combined SAM and ENSO on seasonal Antarctic sea ice changes. The joint SAM–ENSO impacts on southern high latitudes are principally controlled by the strength and position of the wave activity and associated atmospheric circulation anomalies affected by their interactions. In-phase events (La Niña/positive SAM and El Niño/negative SAM) are characterized with an SIC dipole located in the Weddell/Bellingshausen Seas and Amundsen/Ross Seas, while out-of-phase events (El Niño/positive SAM and La Niña/negative SAM) experience significant SIC anomalies in the Indian Ocean and western Pacific Ocean. Sea ice budget analyses are conducted to separate the dynamic and thermodynamic contributions inducing the sea ice intensification anomalies. The results show that in-phase intensification anomalies also display a pattern similar to the SIC dipole and are mainly driven by the direct thermodynamic forcing at the ice edge and thermodynamic responses to meridional sea ice drift in the inner pack, especially in autumn and winter. Dynamic processes caused by zonal sea ice drift also play an important role during out-of-phase conditions in addition to the same mechanisms during in-phase conditions.

KEYWORDS: Antarctica; Sea ice; Antarctic Oscillation; ENSO; Teleconnections

1. Introduction

Sea ice variability has substantial impacts on the exchange of heat and freshwater between atmosphere and ocean (Raphael 2003; Kurtz et al. 2011; Sørensen et al. 2011), ocean circulation (Kirkman and Bitz 2011; Ferrari et al. 2014), local weather systems (Vihma 2014; Smith et al. 2017; Ayres and Screen 2019), and ecosystems (Eicken 1992; Arrigo 2014). Therefore, it is imperative to investigate sea ice variability on different time scales and understand the underlying mechanisms from dynamic and thermodynamic perspectives (Turner and Comiso 2017). In contrast to the rapid decline of the Arctic sea ice extent (SIE) under global warming (Stroeve et al. 2007; Notz and Stroeve 2016; Serreze and Meier 2019), Antarctic SIE trend has displayed a complex pattern since the late 1970s (Parkinson 2019), with a record high in 2014 after long-term increases and then dropping to a record low in 2017 and 2022 (Turner and Comiso 2017; J. Wang et al. 2022; Turner et al. 2022). Therefore, the confidence of the long-term trend is low due to large year-to-year fluctuations (Yuan et al. 2017; Maksym 2019). Current climate models have difficulties simulating this variability precisely (Roach et al. 2020;

Shu et al. 2015), requiring a better understanding of the driving mechanisms.

The dominant interannual variability structure of Antarctic sea ice is characterized by a dipole-like pattern with out-of-phase sea ice anomalies between the Pacific sector and Atlantic sector, called the Antarctic dipole (ADP; Yuan and Martinson 2001). Previous studies have linked the ADP with individual modes of large-scale climate variability like the Southern Annular Mode (SAM), El Niño–Southern Oscillation (ENSO), wavenumber-3 pattern, and semiannual oscillation, among which SAM and ENSO are the primary drivers (Liu et al. 2004; Simpkins et al. 2012; Maksym 2019). The positive phase of the SAM is characterized by an “annular” structure with a deep low pressure anomaly over Antarctica and a high pressure ring surrounding centered near 45°S (Rogers and van Loon 1982; Thompson and Wallace 2000; Fogt and Marshall 2020). The SAM index normally describes the changing intensity and position of westerly winds (Gong and Wang 1999; Thompson and Wallace 2000). Besides, the SAM pattern also contains a zonally asymmetric component, particularly in the Pacific Ocean, strongly connected to tropical variability and zonal wave-3 pattern (Fogt et al. 2012; Fogt and Marshall 2020; Campitelli et al. 2022).

ENSO events also dominantly impact Antarctic sea ice on interannual time scales (Kwok and Comiso 2002; Yuan 2004; Kwok et al. 2016; Zhang et al. 2021). The perturbation of tropical Pacific sea surface temperatures (SST) can affect atmospheric convection, triggering a Rossby wave train propagating southeastward (Hoskins and Karoly 1981; Karoly 1989; Yu et al. 2011). During El Niño (La Niña) events, this stationary wave results in anticyclonic (cyclonic) anomalies over the Amundsen

Supplemental information related to this paper is available at the Journals Online website: <https://doi.org/10.1175/JCLI-D-22-0679.s1>.

Corresponding author: Hao Luo, luohao25@mail.sysu.edu.cn

Sea, leading to a weakening (strengthening) of the climatological Amundsen Sea low (ASL) (Turner 2004; Yuan 2004). Consequently, sea ice will increase (decrease) in the Bellingshausen Sea through cold southerly (warm northerly) winds, and sea ice will decrease (increase) in the Ross Sea through warm northerly (cold southerly) winds (Yuan 2004). This teleconnection has a strong correlation with the large-scale climate variability called the Pacific–South American pattern (Karoly 1989; Mo and Higgins 1998; Yu et al. 2015). The impact of ENSO on Antarctic sea ice is most significant during late austral winter and spring, due to the influence of background atmospheric conditions on the Rossby wave energy propagation (Jin and Kirtman 2009; Song et al. 2011; Simpkins et al. 2012; Yuan et al. 2018). In addition, there are asymmetric impacts between warm (El Niño) and cold (La Niña) ENSO events, stressing the importance of considering the nonlinearity of the sea ice responses (Yuan 2004; Simpkins et al. 2012; Y. Wang et al. 2022). Distinctive impacts also exist between central Pacific (CP) El Niño and eastern Pacific (EP) El Niño on the sea ice in austral spring due to the different locations of their tropical heat sources for atmospheric convection (Zhang et al. 2021). However, there are not enough samples for seasonal analysis during sea ice observations, so the ENSO events are not distinguished into two types in this study.

It is acknowledged that the impact of ENSO on atmospheric circulation at Southern Hemisphere mid–high latitudes depends on the phase of the SAM (L’Heureux and Thompson 2006; Stammerjohn et al. 2008; Fogt et al. 2011). Fogt et al. (2011) revealed that the impact of ENSO is significant only during in-phase conditions, i.e., when La Niña (El Niño) is concurrent with a positive (negative) SAM, or weak SAM conditions. During out-of-phase conditions, i.e., when La Niña (El Niño) is concurrent with a negative (positive) SAM, the impact is largely reduced by the opposing transient eddy momentum fluxes, indicating inverse wave activity fluxes and meridional energy transport in the midlatitudes through eddy–mean flow interactions (Trenberth 1986, 1991). This result is confirmed by Wilson et al. (2016), using the Community Atmospheric Model to assess the El Niño transient eddy dynamics under different SAM regimes. In addition, Gong et al. (2010) suggested that wave breaking characteristics associated with background zonal–mean flow explain the in-phase SAM–ENSO relationship. The correlations between SAM and ENSO are also affected by the type of ENSO (the CP and EP type) and are demonstrated to be more in-phase correlated after the early 1990s (Yu et al. 2015). Therefore, the combination of the SAM and ENSO should have particular influences on Antarctic sea ice through intensified atmospheric and oceanic anomalies. Stammerjohn et al. (2008) investigated the relationship between these combined impacts and the sea ice retreat/advance and showed a similar result to Fogt et al. (2011), with significant sea ice responses particularly in the western Antarctic Peninsula and southern Bellingshausen Sea. Pezza et al. (2012) showed that SAM and ENSO act in synergy on sea ice, with La Niña/positive SAM (LN/pSAM) presenting the most favorable conditions for overall sea ice growth except in the Bellingshausen Sea, using a case of the record-high SIE in summer 2008. However, the record-low Antarctic SIE in summer 2022 is assumed to be

connected with the anomalously deep ASL (Turner et al. 2022; J. Wang et al. 2022), which also happened in the context of a combination of La Niña and pSAM.

However, the seasonal behavior of Antarctic sea ice under each combined SAM and ENSO phase, and their dynamic and thermodynamic contributions, has not been systematically investigated. Investigating these contributions helps us attain a better understanding of the complex feedbacks and interactions giving rise to the sea ice variations. Besides, fine representations of the dynamic and thermodynamic processes controlling sea ice changes are critical for the realistic simulations and reliable predictions of sea ice in climate models. Moreover, few studies pay attention to the influence of these large-scale climate modes on the intensification of sea ice concentration (SIC), which is the rate of sea ice change. We address these questions using the sea ice budget method from Holland and Kwok (2012), where the sea ice intensification is decomposed into advection, divergence, and residual thermodynamic-induced changes. This method has been applied in previous studies to validate whether climate models can produce realistic dynamic and thermodynamic contributions for sea ice evolution (Uotila et al. 2014; Lecomte et al. 2016; Holmes et al. 2019). Holland and Kimura (2016) provided the mean seasonal sea ice budget for the entire Antarctic based on satellite observation data, but the detailed mechanisms concerning local variability were not given. Pope et al. (2017) investigated the impacts of El Niño on the observed sea ice budget of West Antarctica, but they neglected the modulation of the SAM on the relationship between El Niño and Antarctic sea ice and focused merely on the large-scale circulation, without considering local forcings. In this study, the seasonal Antarctic sea ice budget caused by combined ENSO and SAM are examined through their dynamic and thermodynamic processes, and each budget component is further examined with reference to local atmospheric forcings.

The paper is organized as follows. In section 2, the data and method used are outlined. Section 3 presents the results of the climatological backgrounds and the dynamic and thermodynamic contributions to sea ice changes for each SAM–ENSO combination. The main conclusions are summarized in section 4 with further discussion.

2. Data and method

a. Data

We analyze monthly mean sea level pressure (SLP), 10-m wind fields (v_{10}), 850-hPa temperature (T_{850}), mean surface net short-wave (SW; positive downward for all fluxes) and longwave (LW) radiation fluxes, mean surface latent heat (LH) and sensible heat (SH) fluxes, tropical SST (20°N–20°S), 200-hPa geopotential height (Z_{200}), and 200-hPa wind fields from the ERA5 reanalysis (Hersbach et al. 2020). All these variables are retrieved with $0.25^\circ \times 0.25^\circ$ resolution from February 1979 to January 2020. ERA5 is the latest climate reanalysis data produced by the European Centre for Medium-Range Weather Forecasts (ECMWF) and has been widely used in previous studies on the Antarctic (Tetzner et al. 2019; Dong et al. 2020; Zhu

et al. 2021). However, ERA5 slightly underestimates the daily average cloud fraction and shows positive (negative) biases in the shortwave (longwave) radiation effect (Wang et al. 2020; Cerovečki et al. 2022; Hagman 2022), whereas King et al. (2022) pointed out that ERA5 radiation biases are within the measurement uncertainties. Monthly NOAA Extended Reconstructed Sea Surface Temperature version 5 (ERSST v5) data over the same period are used in this study to depict the SST in the Southern Ocean (Huang et al. 2017).

Daily 25-km gridded SIC (Cavaliere et al. 1996) and sea ice drift (SID) (Tschudi et al. 2019) from the National Snow and Ice Data Center (NSIDC) are used for budget analyses. The SIC data are generated from microwave brightness temperature retrievals from the *Nimbus-7* SMMR and DMSP SSM/I-SSM/IS, using the NASA team algorithm. The SID estimates are derived from a merged dataset of different input data sources, including AVHRR, passive microwave data, and NCEP–NCAR reanalysis forecasts. To reduce the noise in ice drift fields and divergence distributions, we smooth the daily SID fields with a 7×7 cell square-window filter following Holland and Kimura (2016).

NOAA Climate Prediction Center (CPC) monthly Antarctic Oscillation (AAO) index and oceanic Niño index (ONI) are used to identify the SAM and ENSO phases, respectively. The AAO index is constructed by projecting the daily 700-hPa height anomalies poleward of 20°S onto the AAO pattern. The ONI is determined by the 3-month running mean of SST anomalies in the Niño-3.4 region (5°N – 5°S , 120° – 170°W). The ONI is first multiplied by -1 so that a positive ONI denotes a La Niña event and vice versa. These indices are detrended and standardized, and thresholds of ± 0.5 are set to distinguish the four SAM–ENSO combinations, as shown in Fig. 1, following Fogt et al. (2011). Here, we assume that the removed linear trend of the AAO index is the anthropogenic component forced by ozone and greenhouse gases (Thompson and Solomon 2002).

b. Budget analysis

The SIC budget equation originates from Holland and Kwok (2012):

$$\frac{\partial C}{\partial t} = -\nabla \cdot (\mathbf{u}C) + \text{residual}, \quad (1)$$

where C is the sea ice concentration and \mathbf{u} is the sea ice drift. The term $\partial C/\partial t$ is referred to as sea ice intensification and is calculated as a central difference between SIC from the day after and before. The $-\nabla \cdot (\mathbf{u}C)$ term represents the dynamic components, including advection and divergence processes. Daily dynamic terms are calculated using central differences in space and then smoothed with 3-day average. The residual term includes the contributions from thermodynamic freezing or melting and mechanical redistributions like ridging and rafting. The signs in Eq. (1) are chosen to guarantee that positive values are connected to increased sea ice concentration. Following the criterion in Holland and Kimura (2016), we consider that ridging and rafting

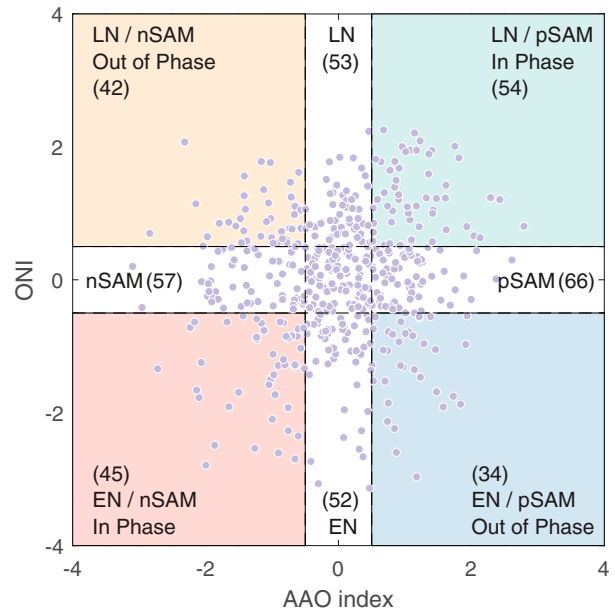


FIG. 1. Combinations of regimes based on AAO index and ONI. ONI is inverted and both indices are detrended and standardized. Each purple circle represents a month. Numbers of each circumstance are given in the parentheses. The combination of La Niña (El Niño) and positive (negative) SAM is abbreviated to LN/pSAM (EN/nSAM) and the rest are similar.

may exist within the residual where the residual term is negative, SID is convergent, and SIC is high ($>90\%$); otherwise, the residual is considered to represent thermodynamic processes.

c. Surface heat flux

Since Eq. (1) is unable to fully distinguish the contributions from thermodynamic and mechanical processes, and in order to investigate the influence of local forcing which contributes to a majority of surface temperature variations during thermodynamic processes, we composite the surface heat flux parameters for each SAM–ENSO combination and each season. Net surface heat flux depends on radiation fluxes and turbulent heat fluxes, specifically determined by Eq. (2):

$$F_{\text{net}} = LW_{\text{net}} + SW_{\text{net}} + H_s + H_l, \quad (2)$$

where F_{net} is the net surface heat flux, LW_{net} and SW_{net} are mean surface net longwave and shortwave radiation fluxes, and H_s and H_l are mean surface sensible and latent heat fluxes, respectively.

d. Methodology

We apply composite analysis to examine the anomaly fields, and each SAM–ENSO combination is defined in Fig. 1, using the Wilcoxon rank sum statistical significance test (Pettitt 2014) to detect whether the composite fields are significantly different from climatology. Each purple circle represents a month. The monthly anomalies are calculated relative to

TABLE 1. The total numbers of samples under each SAM–ENSO combination in each season; the numbers of different years those samples come from are given in the parentheses. The combination of La Niña (El Niño) and positive (negative) SAM is abbreviated to LN/pSAM (EN/nSAM) and the rest are similar.

	Summer (FMA)	Autumn (MJJ)	Winter (ASO)	Spring (NDJ)
LN/pSAM	9 (8)	11 (8)	10 (8)	24 (11)
EN/nSAM	6 (5)	10 (6)	9 (8)	20 (12)
LN/nSAM	7 (7)	8 (6)	14 (10)	13 (8)
EN/pSAM	7 (4)	7 (6)	10 (8)	10 (8)

monthly mean climatology based on 1979–2020 in order to remove the seasonal cycle, and then composited for each season and each combination. Composite analysis can provide better insight into the ENSO teleconnection variations compared with correlation analysis (Fogt et al. 2011). We define each austral season on the principle that winter is centered on the month of maximum SIC according to Holland and Kimura (2016), i.e., winter covers August, September, and October (ASO). This kind of seasonal division can provide sufficient samples in each SAM–ENSO combination for composite analysis (Table 1). However, it is noted that the “summer” season defined here includes a month of sea ice growth (April) due to the asymmetry of the Antarctic sea ice seasonal cycle.

3. Result

a. Rossby wave train induced by SAM–ENSO interactions

Previous studies have demonstrated the mechanisms of the variations in the ENSO teleconnection intensity under different SAM–ENSO combinations (Gong et al. 2010; Fogt et al. 2011; Wilson et al. 2016). Fogt et al. (2011) revealed that the effects of the teleconnections are connected to interactions between ENSO-induced and SAM-induced transient eddy momentum flux. During in-phase conditions, the transient eddy momentum fluxes act in synergy with each other over the South Pacific, and consequently anomalous transient momentum flux convergence acts to amplify the zonal wind anomalies and maintain the ENSO teleconnections (see Fig. 12 in Fogt et al. 2011). During out-of-phase conditions, they oppose each other, impeding the ENSO signals reaching the South Pacific. These interactions finally affect the wave propagation and breaking and zonal wind anomalies.

Here, we examine the teleconnection associated with tropical SST anomalies and Takaya–Nakamura (T–N) wave activity fluxes (TN01 for short) for each season under different SAM–ENSO combinations. TN01 is a diagnostic tool to demonstrate the propagating stationary Rossby wave train (Takaya and Nakamura 2001) and is calculated using geopotential fields and wind fields in 200 hPa. Figure 2 shows the composites of 200-hPa geopotential height anomalies, tropical SST anomalies, and TN01. It is obvious that during in-phase conditions [LN/pSAM and El Niño/negative SAM (EN/nSAM)] the teleconnections

from the tropics are robust and strong pressure anomalies are established in the South Pacific sector, consistent with the conclusions of previous studies (Gong et al. 2010; Fogt et al. 2011; Wilson et al. 2016). The established geopotential height anomalies peak in winter during in-phase events, agreeing with previous studies that ENSO influence peaks during late austral winter and spring (e.g., Jin and Kirtman 2009; Ding et al. 2012; Yiu and Maycock 2019), since we define winter as ASO here. The asymmetries between LN/pSAM and EN/nSAM originate from wave propagation and the tropical heating regions as noted by a few studies before (e.g., Welhouse et al. 2016; Wang et al. 2021), with TN01 showing strong southward propagation in summer in the South Pacific during EN/nSAM, compared with weaker TN01 there during LN/pSAM. During out-of-phase conditions, wave propagations are weakened and distinct pressure anomalies are located over the eastern Antarctic continent and also extend to the western Pacific Ocean and Indian Ocean.

b. Climatological background

Based on the results of wave activity anomalies, we examine the composite distributions of atmospheric and oceanic anomalies including SLP, v_{10} , T_{850} , SST, SIC, and SID under each SAM–ENSO combination.

In the LN/pSAM condition, there are significant seasonal variations for all the anomalies (Fig. 3). The SLP presents low pressure anomalies over the high-latitude Southern Hemisphere and a marked low pressure center in the eastern Pacific sector, which deepens the ASL (Figs. 3a–d), in line with what Fogt et al. (2011) discovered. These local anomalies grow stronger from summer to winter, and then become weaker in spring, consistent with the teleconnection variations. The position of the low pressure center moves onshore after summer. Induced by the SLP anomalies, v_{10} presents intensified westerly winds and cyclonic winds around the low pressure (Figs. 3e–h). However, significant meridional wind anomalies (black vectors) only exist in the northerly winds toward the Antarctic Peninsula and southerly winds over the Ross Sea. Due to the meridional wind anomalies, midlatitude heat and moisture are transported poleward in the Atlantic sector and equatorward in the Pacific sector, resulting in a distinct temperature dipole particularly in autumn and winter. Aligned with the northerly (southerly) flow and warm (cold) overlying atmosphere, SST anomalies present a Bellingshausen–Ross Sea dipole. However, winter SST anomalies do not perfectly match the pattern of the v_{10} , T_{850} , and F_{net} fields (Figs. 3c,g and 7o), in particular showing little response to the strongest wintertime atmospheric anomalies (Fig. 3k). Note that the standard deviations of SST anomalies in the winter Ross Sea are large (not shown). Other SST products (ECMWF Ocean Reanalysis System 5, NOAA Optimal Interpolation SST Analysis) are tested, and the same results are achieved, indicating that other oceanic processes like Ekman heat fluxes and storm perturbations also play a critical role in the ocean’s response (Sen Gupta and England 2006; Ciasto and England 2011; Wilson et al. 2019). Easterly (westerly) wind anomalies cause poleward (equatorward) transports of warm (cold) water and thus positive

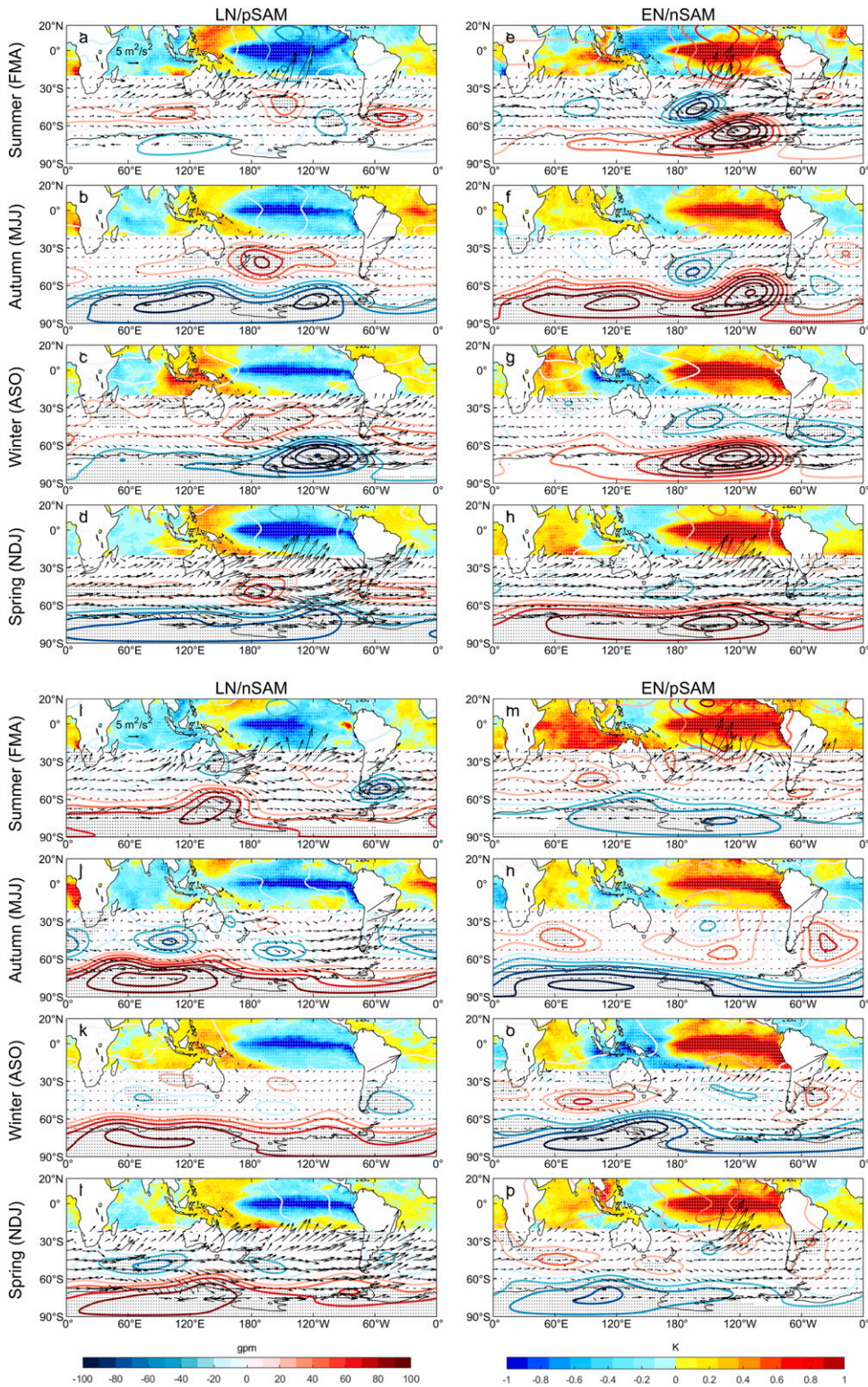


FIG. 2. Composites of 200-hPa geopotential height anomalies (contours), tropical SST anomalies (shading), and T-N wave activity fluxes (vectors) of each season and each SAM-ENSO condition: (a)–(d) LN/pSAM, (e)–(h) EN/nSAM, (i)–(l) LN/nSAM, and (m)–(p) EN/pSAM. The black dots represent geopotential height values passing the 95% significance test and white dots for SST values.

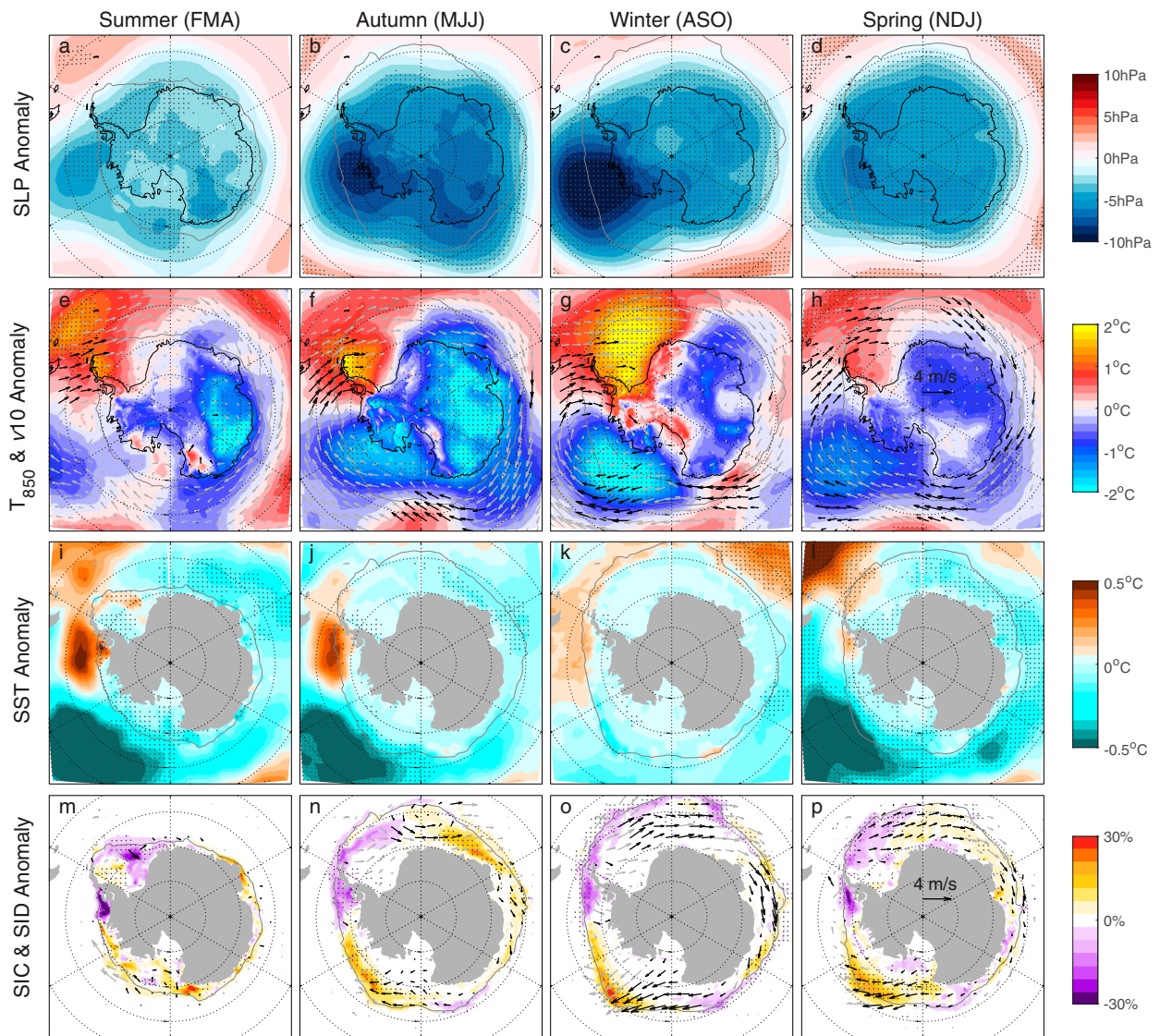


FIG. 3. Composites of SLP, v_{10} , T_{850} , SST, SIC, and SID anomalies for each season in the LN/pSAM condition. The gray contour indicates the 15% SIC climatology for each season during 1979–2019. The dots indicate the shaded values passing the 95% significance test. The black vectors indicate the meridional wind and SID values passing the 95% significance test while the gray vectors do not.

(negative) Ekman heat flux anomalies (Yeo and Kim 2015). These oceanic contributions warrant further investigations.

Consequently, SIC anomalies also present a dipole under the influences of both atmospheric and oceanic processes, with negative anomalies in the Bellingshausen/Weddell Sea and positive anomalies in the Amundsen/western Ross Sea. Weaker but significant positive SIC anomalies exist in the Indian Ocean and western Pacific Ocean as well, in concert with the findings of Yadav et al. (2022). The effects are confined at the ice edge in winter but extend to the inner ice pack in other seasons. As shown in Figs. 3m–p, SID anomalies basically coincide with wind anomalies and point at a small angle to the left of the wind vectors caused by Ekman drift. SID anomalies present significant eastward drifts in the eastern Weddell Sea and Indian

Ocean, and northward drifts in the northern Ross Sea. The largest SID anomalies exist in winter, corresponding to SLP and wind anomalies. Moreover, the high correlations between the v_{10} and SID in most regions are verified through a vector correlation method (not shown; Crosby et al. 1993). Compared with the SAM-only and ENSO-only impacts (Figs. S1, S2 in the online supplemental material) generated by partial correlation analysis (Stuart et al. 2009), we find that when the two modes take effect together, SLP anomalies are more reflective of the SAM, and SST anomalies are more reflective of ENSO. The reason for this phenomenon still needs further investigations from the perspective of oceanic processes.

In the EN/nSAM condition, which is also an in-phase combination, the anomalies are generally opposite to those in

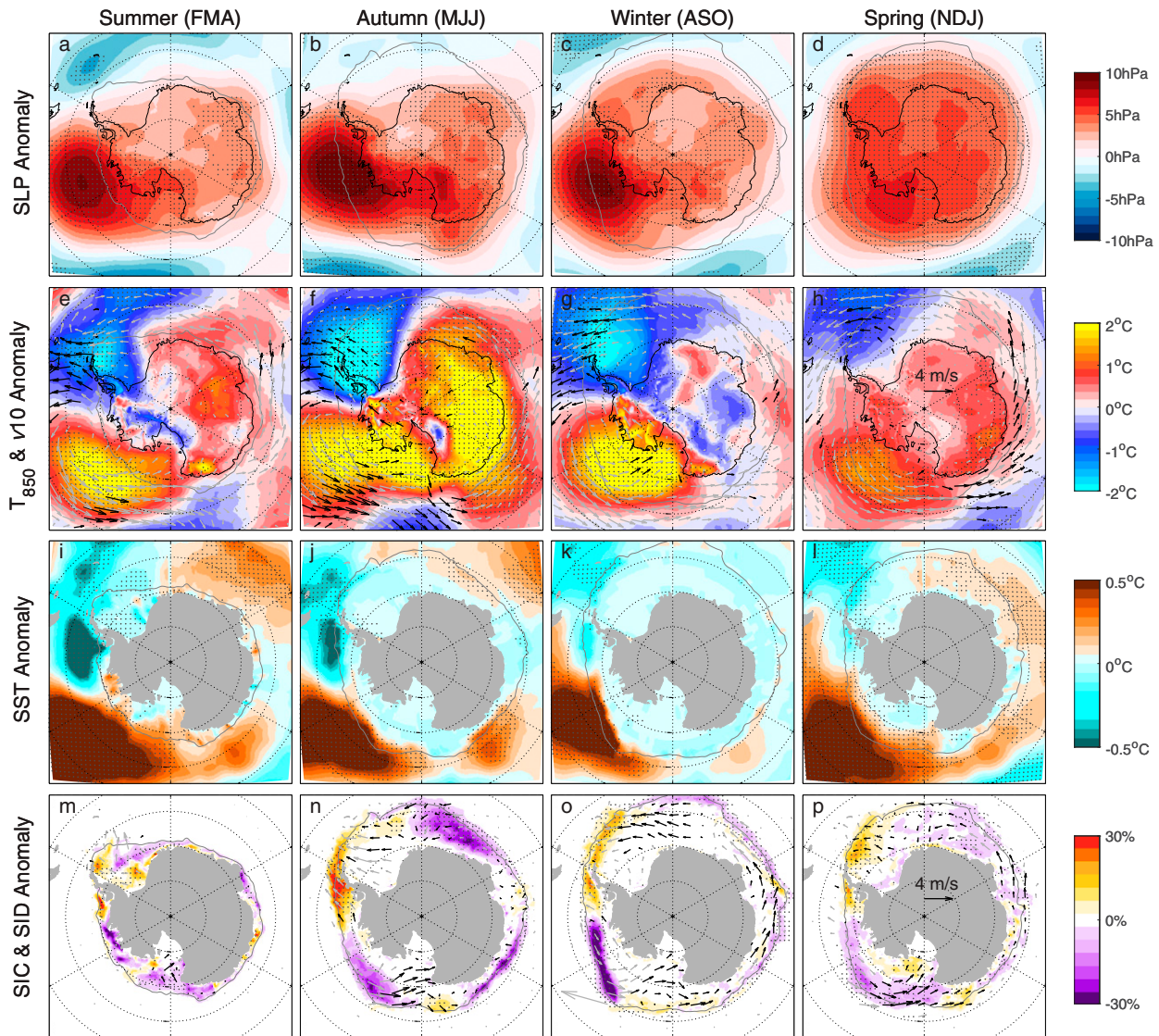


FIG. 4. As in Fig. 3, but for the EN/nSAM condition.

Fig. 3, as shown in Fig. 4. A notable difference is that the SLP and T_{850} anomalies are stronger in summer compared with LN/pSAM conditions, and they peak in autumn rather than winter (Fig. 4b), revealing a seasonal asymmetry between two in-phase relations. Strong positive SST anomalies in the eastern Pacific occur in all seasons (Figs. 4i–l), and the winter anomalies are in contrast to LN/pSAM conditions. Meanwhile, SIC anomalies in EN/nSAM conditions are much stronger in autumn and winter. Significant SID anomalies present opposite distributions to LN/pSAM conditions, which are westward drifts in the Weddell Sea and Indian Ocean and southward drifts in the Ross Sea, and the strength of the SID anomalies is weaker in EN/nSAM winter.

The anomalies are apparently different in the La Niña/negative SAM (LN/nSAM) condition, one of the out-of-phase relations (Fig. 5). The consistent positive SLP anomalies cover the whole

Antarctic continent and extend to the western Pacific Ocean and Indian Ocean. Seasonal differences still exist, with SLP anomalies more annular in winter and spring compared with summer and autumn. Therefore, the primary wind anomalies are the easterly winds around the anomalous high pressure, with significant northward winds in the Indian Ocean and northern Ross Sea. The air temperature anomaly dipoles disappear, and significant anomalies only exist over the continent and the western Pacific Ocean. Although not significant, negative T_{850} anomalies are located in the western Weddell Sea, and positive anomalies along the coast of West Antarctica. Positive SST anomalies are located to the east relative to the T_{850} anomalies and are stronger in autumn and spring, probably due to oceanic heat advection toward the east. The SIC anomalies do not present the dipole patterns as in-phase conditions, but are basically consistent with SST anomalies, showing significant SIC anomalies in the Indian Ocean and

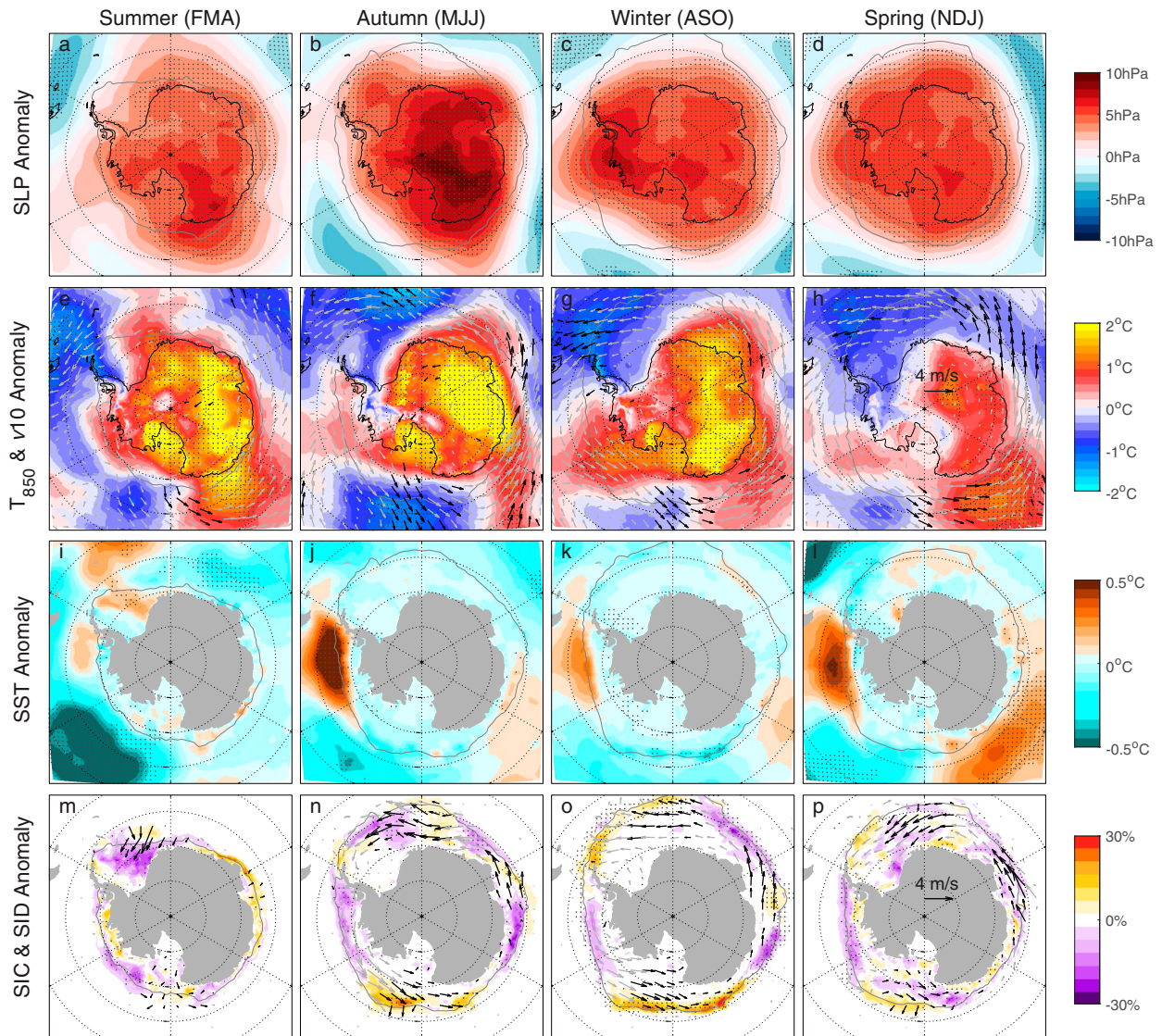


FIG. 5. As in Fig. 3, but for the LN/nSAM condition.

western Pacific Ocean. Compared with EN/nSAM (Fig. 4), significant SID anomalies display similar westward drifts in the Weddell Sea and Indian Ocean but northward drifts in the Ross Sea, implying that ENSO controls sea ice changes in the Ross Sea while the eastern Weddell Sea is affected by SAM.

In the El Niño/positive SAM (EN/pSAM) condition, the anomalies are similar to Fig. 5 but with opposite signs (Fig. 6). Negative SLP anomalies exist in the Indian Ocean and western Pacific Ocean, accompanied by westerly wind anomalies. Few T_{850} anomalies over the Southern Ocean are significant, with insignificant positive anomalies located in the western Weddell Sea and negative anomalies in the western Pacific sector. Positive SST anomalies move westward to the northern Amundsen Sea compared with LN/nSAM conditions. Significant and stronger SIC and SID anomalies occur, opposite to the distribution in LN/nSAM conditions. The generally eastward drifts also have a

northward component in the Weddell Sea and a southward component in the Ross Sea in winter.

These analyses reveal that SIC has different seasonal responses under different SAM–ENSO combinations, affected by both atmosphere and ocean, which cannot be regarded as linear sums between ENSO and SAM events. In-phase conditions mainly have influences on the Atlantic–eastern Pacific sectors and out-of-phase conditions on the western Pacific–Indian sectors. Compared with SAM- and ENSO-only events, SAM exerts more important impacts on SLP and T_{850} in the SAM–ENSO combination, while ENSO is more important to SST. Moreover, the effects of ENSO are more distinct in the South Pacific, while SAM influences are widespread in the Southern Ocean. To further understand the driving mechanisms of the SIC anomalies, the dynamic and thermodynamic contributions to the SIC budget are now examined.

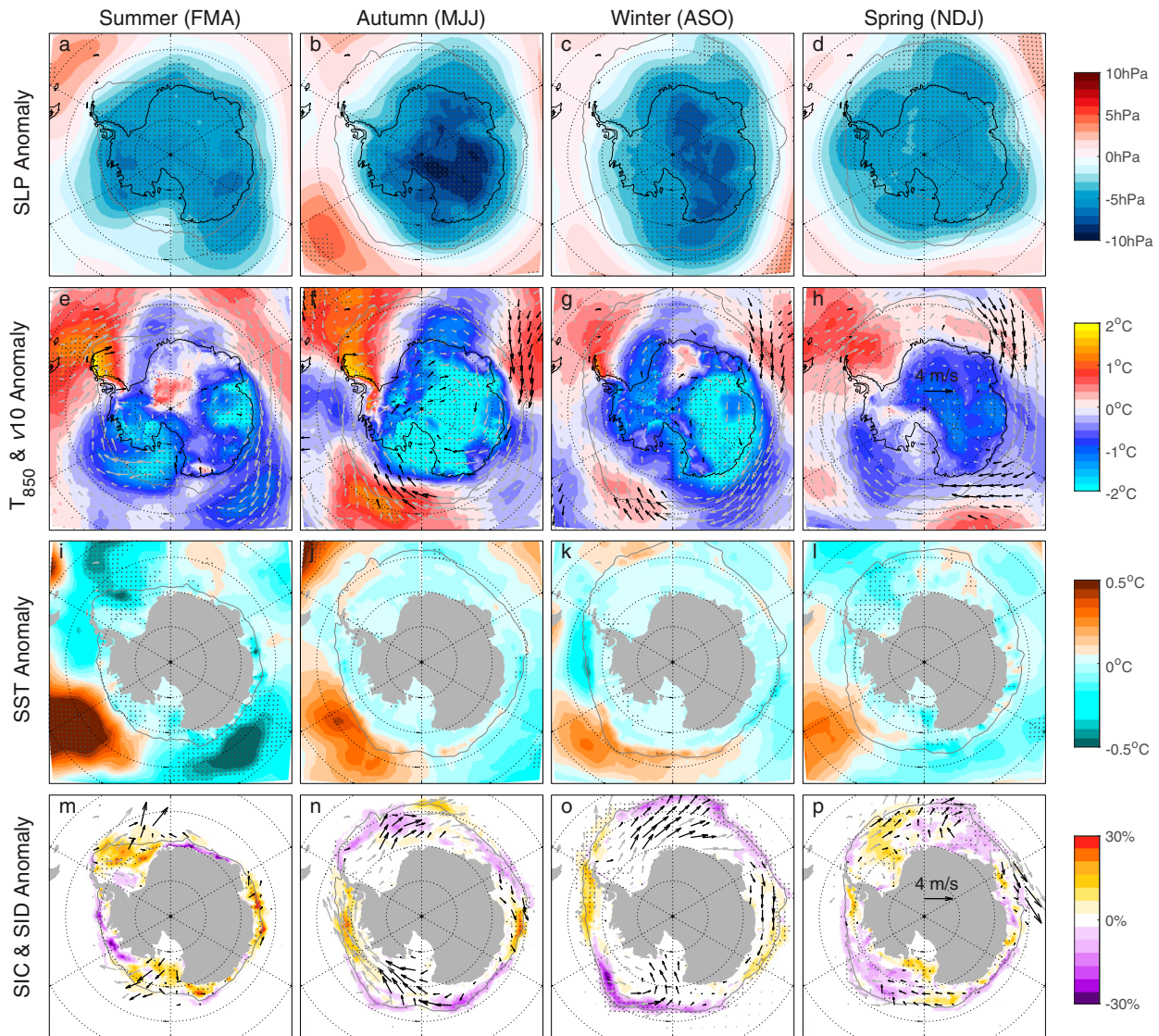


FIG. 6. As in Fig. 3, but for the EN/pSAM condition.

c. Budget analysis

We employ the SIC budget equation [Eq. (1)] to analyze the dynamic and thermodynamic contributions to the daily SIC intensification anomalies. Composite analyses are conducted for the budget terms in each combination of SAM and ENSO. The residual terms include both thermodynamic contributions and mechanical redistribution. However, they are dominated by thermodynamic processes according to previous studies (Holland and Kwok 2012; Holland and Kimura 2016; Pope et al. 2017), and the regions where ridging is likely to happen are shown in Figs. 7–10. It is noted that the dynamic patterns cannot cover all of the sea ice intensification, especially in summer, because of the missing ice drift data mostly at the ice edge in the Pathfinder product (Holland and Kimura 2016). Meanwhile, only the grid cells of intensification

and thermodynamic fields where dynamic fields are valid are shown to maintain consistency among the different terms.

For LN/pSAM conditions, the dominant contributions vary from season to season. The sea ice intensification anomaly in summer is represented mainly by the residual component (Figs. 7a,i), showing a significant positive intensification in the central Weddell Sea, i.e., more sea ice is produced here. Except for a small region near the coast of the Antarctic Peninsula, the residual term is primarily dominated by thermodynamic processes. In autumn and winter, intensifications grow larger and display a dipole between the Atlantic Ocean and eastern Pacific Ocean, as shown in Figs. 3n and 3o. Dynamic processes including divergence and advection cause a similar magnitude of contributions as thermodynamic processes. Specifically, divergence anomalies mainly cause intensification in the inner pack, while advection anomalies cause

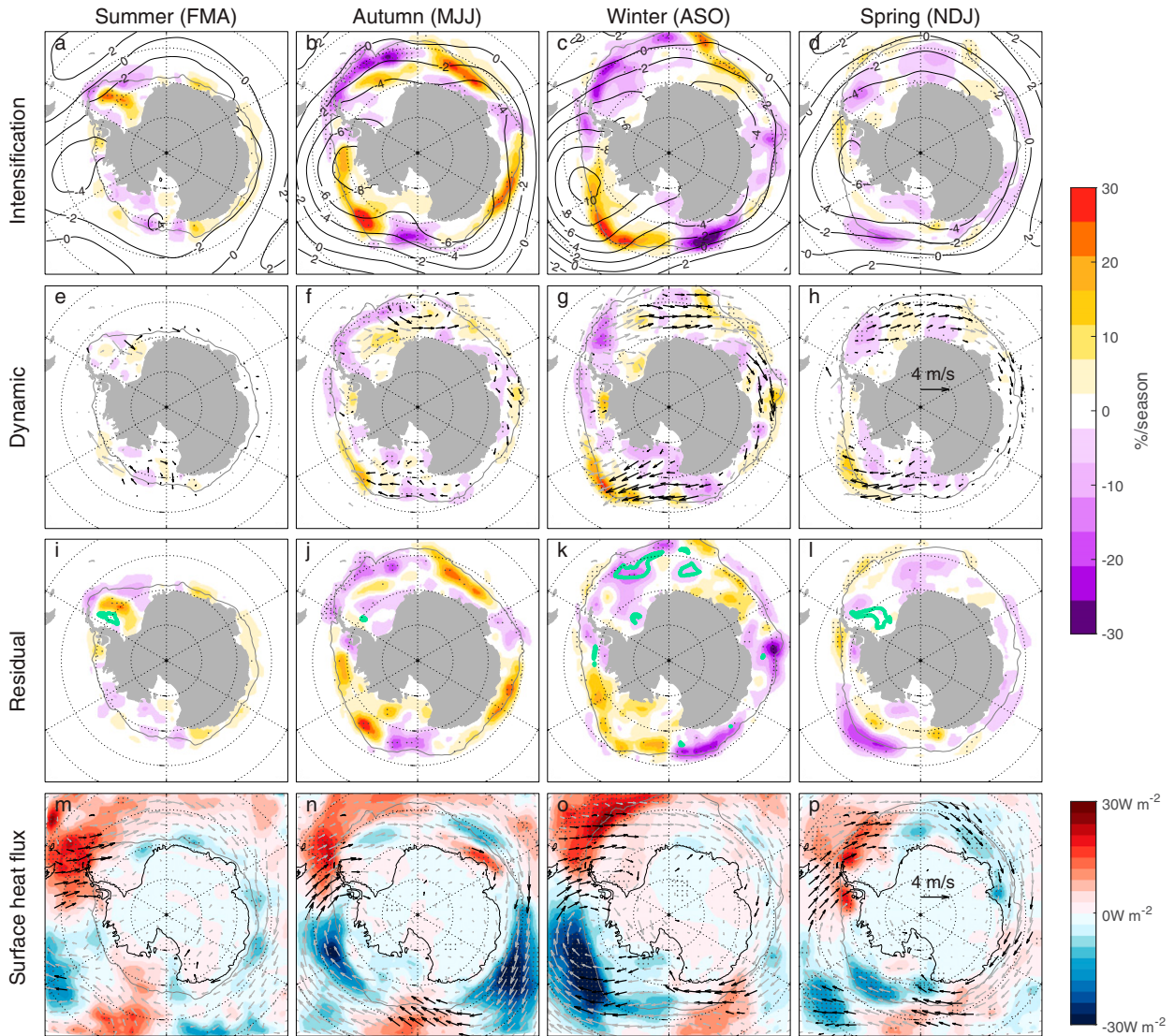


FIG. 7. (a)–(l) SIC budget anomaly composites (shading) in the LN/pSAM condition for each season. The dots represent values passing the 95% significance test. The gray contour indicates the 15% SIC climatology for each season during 1979–2019. The black contours in (a)–(d) represent the corresponding SLP anomalies. The black vectors in (e)–(h) indicate the meridional SID values passing the 95% significance test while the gray vectors not. The green contours in (i)–(l) represent the regions where ridging is likely to dominate the residual based on the criterion of negative residual, convergent SID, and SIC > 90%. (m)–(p) F_{net} anomalies composites (shading) in the LN/pSAM condition for each season. The black dots represent values passing the 95% significance test. The black vectors indicate the meridional wind values passing the 95% significance test while the gray vectors do not.

decreased SIC in the Weddell/Bellingshausen Seas and increased SIC in the Amundsen/Ross Seas and eastern Antarctic at the ice edge (not shown). The effects of divergence/advection on inner/ice edge regions have also been proved in [Holland and Kimura \(2016\)](#). Due to the strong negative SLP anomalies in the Amundsen Sea (Figs. 3b,c), warm air blows southward in the Weddell Sea and Bellingshausen Sea, while cold air blows northward in the Amundsen Sea and Ross Sea. Significant northward SID anomalies in the Ross Sea induce negative anomalies onshore and positive ones offshore (Figs. 7f,g), accompanied by positive thermodynamic freezing (Figs. 7j,k). At the ice edge the freezing

processes come from strong cold anomalies, while in the inner pack they are induced by the exposure to cold atmosphere due to the divergent ice drift. The situation is a little different in the Weddell Sea, where southward warm air compacts and melts sea ice simultaneously, including in the area where mechanical redistribution is possible.

In spring, sea ice starts to melt, so we assume that intensification anomalies result mainly from thermodynamic processes. Inner pack sea ice flows outwards in the Weddell Sea and Ross Sea and melts at the ice edge. Comparing the F_{net} anomalies (Figs. 7m–p) with the residual anomalies (Figs. 7i–l), positive

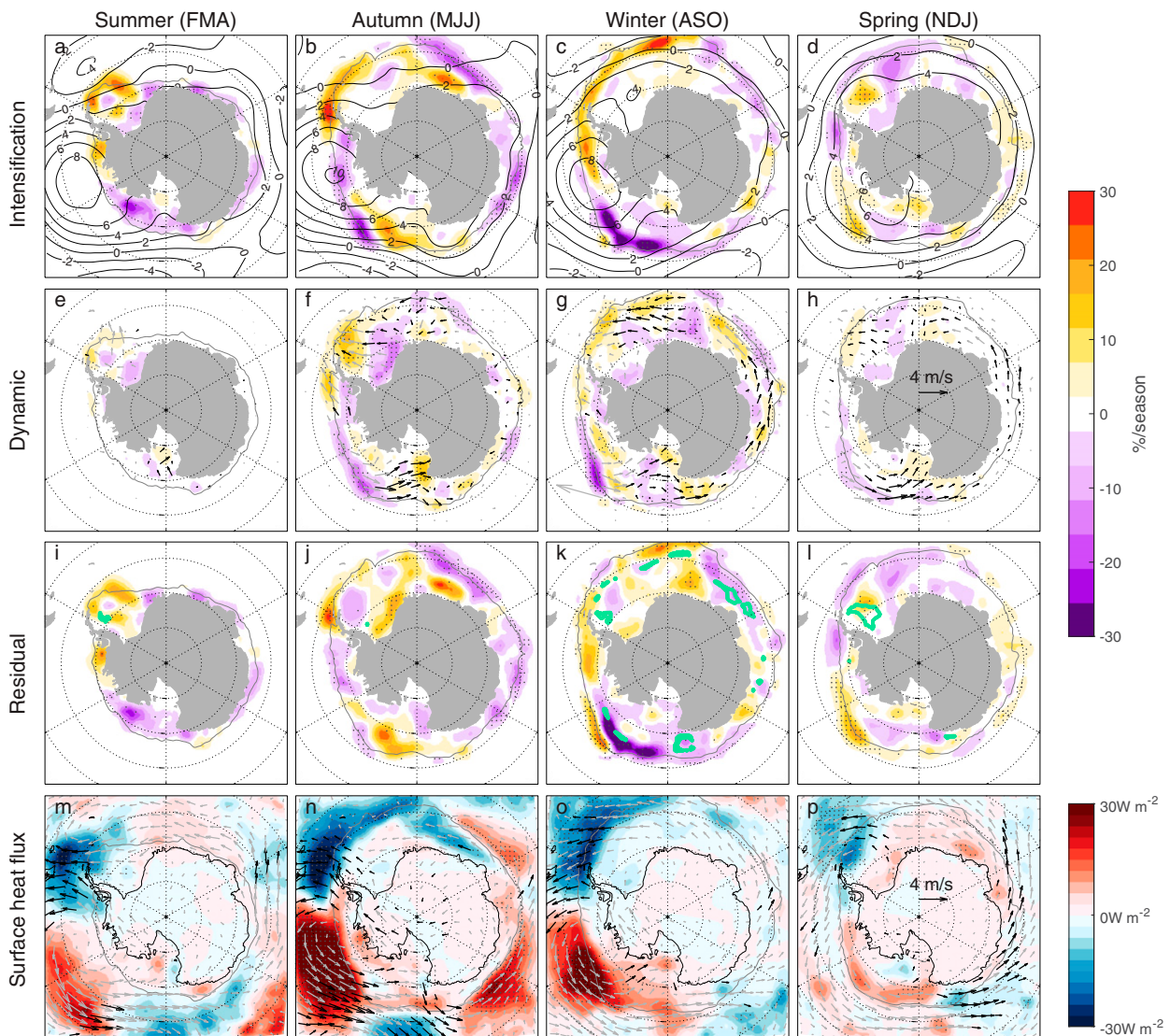


FIG. 8. As in Fig. 7, but for the EN/nSAM condition.

F_{net} anomalies generally correspond to negative sea ice intensification and vice versa. Tracing the sources of the F_{net} , we find that SW_{net} are the prominent source of thermodynamic processes in spring (Fig. S3). During this melting season, increased SW anomalies due to reduced low cloud cover and more medium-height cloud cover (not shown) lead to sea ice loss and decreased albedo (retrieved from ERA5) and consequently result in more SW absorption and more sea ice melting. The H_s and H_l anomalies contributing to sea ice variations are of a magnitude similar to SW and LW anomalies through all seasons. Oceanic heat exchanges are also important to SIC variations, but they are not investigated in this study and still need further examination in the future.

Sea ice intensification in EN/nSAM conditions shows significant negative anomalies in the Amundsen/Ross Seas and positive anomalies in the Weddell Sea in all seasons except spring (Figs. 8a–d), consistent with the seasonal variability of SIC

anomalies (Figs. 4m–p). The position of the intensification dipole between the Atlantic and Pacific sectors moves westward in winter compared with autumn (Figs. 8b,c). Northward (southward) drift anomalies in the Weddell Sea (Ross Sea) and accompanying freezing (melting) anomalies in autumn contribute to the dipole anomalies together, while thermodynamic processes give rise to anomalies in the eastern Antarctic. Similar situations happen in winter, along with the frequent possibility of mechanical redistributions around Antarctica (Fig. 8k). The spring intensifications are composed of more significant positive anomalies compared with LN/pSAM, which may come from the thermodynamic feedback suggested by Pope et al. (2017) that sea ice melts earlier here in winter, since T_{850} and SST anomalies do not obviously explain the thermodynamic forcings. In EN/nSAM conditions, F_{net} anomalies are nearly opposite to LN/pSAM and coincide with T_{850} anomalies (Figs. 4e–h). The magnitude of SW and LW anomalies is significantly larger than

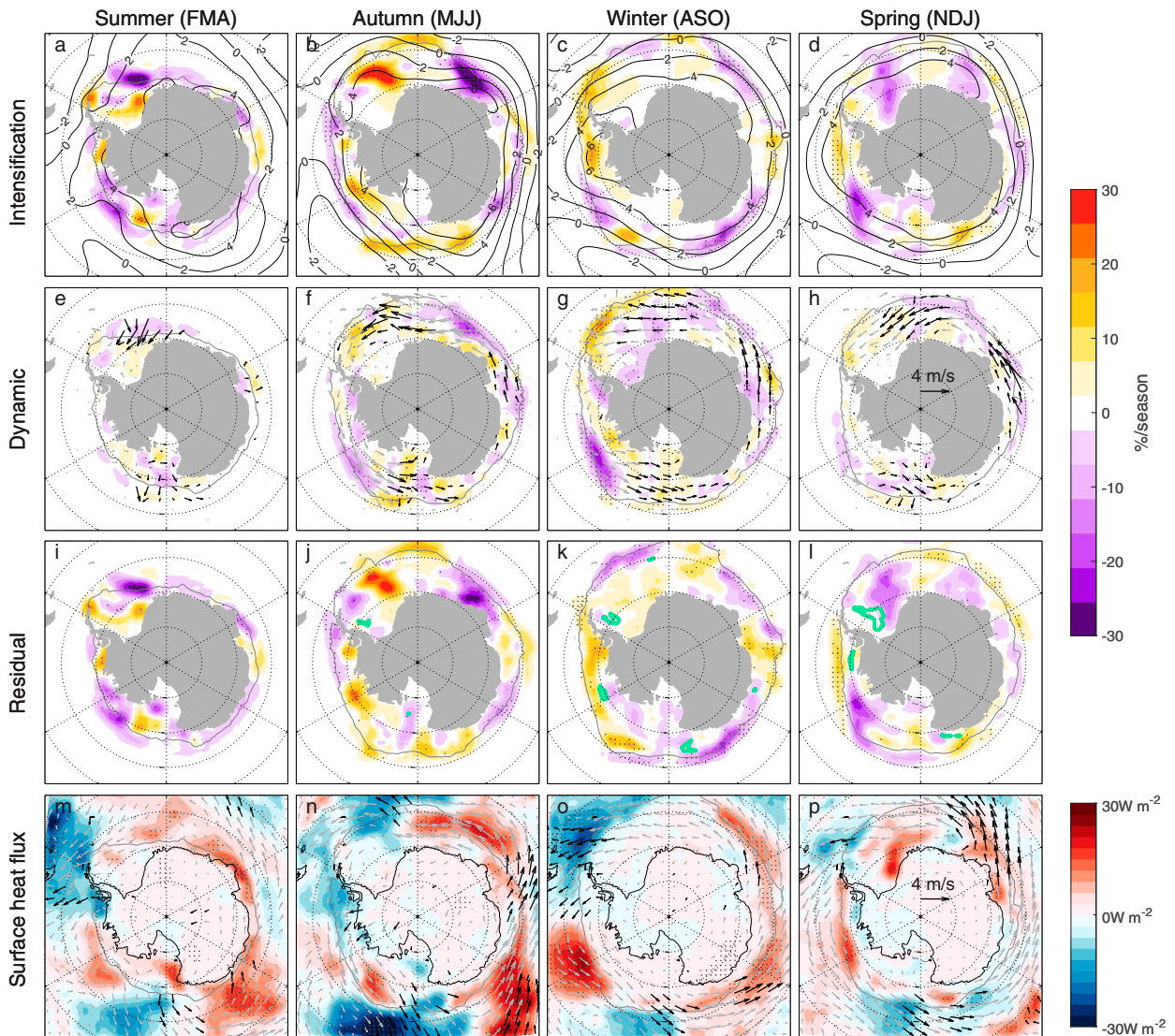


FIG. 9. As in Fig. 7, but for the LN/nSAM condition.

LN/pSAM in summer (Fig. S4), and both radiation anomalies oppose each other in the Amundsen/Ross Seas. Consequently, the summer heat fluxes are contributed by H_s and H_l .

Compared with in-phase conditions, dynamic effects play a more important role in summer during LN/nSAM, since the SID anomalies are stronger in the Weddell Sea and Ross Sea (Fig. 9). The clear dipole anomalies in West Antarctica in autumn and winter disappear. Nevertheless, dynamic terms still matter in a different way. The autumn opposing anomalies in the Weddell Sea and Indian Ocean are caused by convergence and advection induced by westward drift, respectively, and are also associated with the thermodynamic effects shown in F_{net} . The anomalies in H_s and H_l are notably weaker than in-phase relations (Fig. S5). Similar mechanisms underlie the opposing anomalies between the Amundsen Sea and Ross Sea, which indicates annular SAM-like dynamics, i.e., zonal advection of sea ice, are important to sea ice changes. Spring

intensification anomalies indicate more ice decrease in the Weddell Sea and Amundsen Sea as well as less decrease in the Bellingshausen Sea and are controlled generally by thermodynamic forcings.

In EN/pSAM, thermodynamic processes cause a general sea ice increase in summer, except in some regions near the Antarctic Peninsula and western Pacific Ocean, while dynamic processes decrease sea ice in the western Weddell Sea and southern Ross Sea and increase sea ice in the northern Ross Sea (Figs. 10a,e,i). The intensifications in autumn present a circle of negative anomalies at the ice edge and opposite inside, contributed mainly by thermodynamics, with melting anomalies at the ice edge from the surface heat flux and cold freezing anomalies inshore. Mechanisms are similar in winter but result in different spatial distributions due to different F_{net} forcings. Spring intensification anomalies are larger than in-phase conditions and resemble residual and heat flux

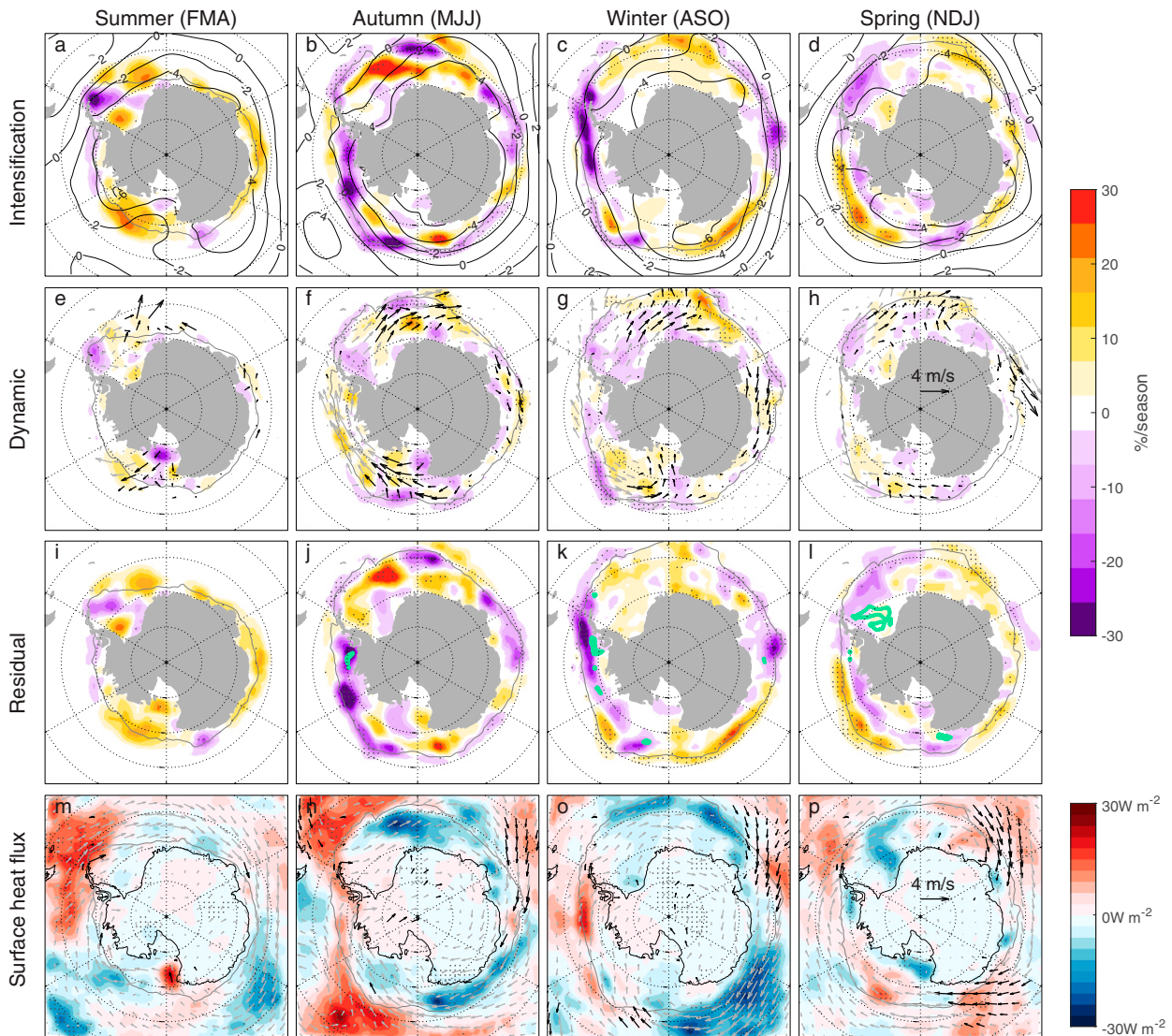


FIG. 10. As in Fig. 7, but for the EN/pSAM condition.

patterns, mainly caused by thermodynamic contributions and especially SW_{net} (Fig. S6).

4. Summary and discussion

This study targets the impacts of combined SAM and ENSO on Antarctic seasonal sea ice changes. Two kinds of events are defined based on the monthly SAM–ENSO standardized indices, including in-phase events (LN/pSAM and EN/nSAM) and out-of-phase events (LN/nSAM and EN/pSAM).

During in-phase conditions, the teleconnections between the tropics and high latitude in the Southern Hemisphere are robust, and pressure anomalies occur in the South Pacific sector characterized by distinct SLP anomalies in the Amundsen Sea. The 10-m wind speed presents corresponding anomalies, and consequently SIC anomalies also present a dipole between the Weddell/Bellingshausen Seas and the Amundsen/Ross Seas

in all seasons except summer. SIC anomalies are primarily affected by SAM-induced atmospheric anomalies and ENSO-induced oceanic anomalies. Analyzing the sea ice budget, we find that thermodynamic and dynamic processes contribute together to intensification anomalies in autumn, winter, and spring, while thermodynamic processes dominate in summer. A common mechanism is that northward drift induces negative anomalies onshore and positive anomalies offshore, accompanied by positive thermodynamic freezing anomalies onshore. In contrast, southward drift is associated with sea ice compacting and melting simultaneously, even leading to possible mechanical redistribution. SW_{net} dominates F_{net} in spring, but H_s and H_l are the primary drivers in other seasons.

During out-of-phase conditions, Rossby wave propagation is weakened, and the anomalies are focused on the western Pacific Ocean and the Indian Ocean, leading to zonal wind anomalies around the anomalous pressure centers. The SIC

anomalies present no dipole patterns but are basically consistent with temperature anomalies. In addition to the dynamic and thermodynamic mechanisms mentioned above, dynamic processes caused by zonal sea ice drift and associated thermodynamic responses also play an important role during out-of-phase conditions.

Since a composite analysis is used to achieve a general relation between ENSO–SAM combinations and sea ice change, interannual variability is masked. Therefore, we examine the time series of the MSLP, SIC, and sea ice intensification anomalies for the eastern Pacific Ocean (Indian Ocean) during in-phase (out-of-phase) events, as shown in Fig. S7 (Fig. S8). We find that one specific event generally lasts for a short time, ranging from 1 to 5 months. Sometimes a longer period is dominated by a specific event, though not continuously. During in-phase conditions, most LN/pSAM events correspond to negative MSLP anomalies and positive SIC anomalies, which is the opposite for EN/nSAM. The weaker responses in sea ice intensification anomalies can be attributed to the strong seasonality and meridional compensation of the signals (Figs. 7 and 8). Meanwhile, the Indian Ocean responses to out-of-phase events are more notable for MSLP anomalies, owing to the strong asymmetries between LN/nSAM and EN/pSAM effects on sea ice.

One assumption used in the event classification is that SAM and ENSO are considered two independent Antarctic climate modes, supported by Fig. 1. Nevertheless, the ONI that represents average SSTs across the tropical Pacific might mask the internal connection between the two modes (Seager et al. 2003; Zubiurre and Calvo 2012; Ding et al. 2012). Seager et al. (2003) revealed a mechanism connecting ENSO and extratropical climate through changes in the subtropical jets, the transient eddies, and the eddy-driven mean meridional circulation. Zubiurre and Calvo (2012) found that El Niño Modoki events can induce a winter Antarctic stratosphere warming, and a downward-propagating signal contributing to SAM in spring. Ding et al. (2012) suggested that the SAM is correlated with tropical eastern and central Pacific SST in summer, while only with the latter in winter. In fact, the combined effect of SAM and ENSO in this study contains the SAM–ENSO interrelationship. That is, a month when both the standardized AAO index and ONI are larger than 0.5 indicates that strong positive SAM and strong La Niña happen together, while the strong positive SAM could be influenced by the strong La Niña and vice versa. Therefore, our paradigm is not contradictory to the paradigm of previous studies but agrees with some of their findings. As Ding et al. (2012) demonstrated, the Pacific sector variability is related to tropical forcing and the Indian sector variability is related to midlatitude dynamic processes. This conclusion supports our results that in-phase events lead to significant anomalies in the Pacific Ocean while out-of-phase events cause the Indian Ocean anomalies.

Apart from the SAM-accompanied pressure and wind anomalies, the “two-time-scale” response of sea ice to SAM may also matter (Ferreira et al. 2015; Hobbs et al. 2016; Doddridge and Marshall 2017). After a short-term ocean cooling response and sea ice expansion, sustained SAM-induced westerly winds could result in upwelling of warmer water due to Ekman drift and sea

ice loss. However, Polvani et al. (2021) demonstrated that SAM only explains 14% of the sea ice trend during the ozone depletion period and is not the primary driver of sea ice trends. Therefore, we assume that the effects of slow SAM–ocean processes on sea ice are small compared with the synchronous impacts. Further studies should investigate this issue through lagged composites or regression in the future.

Our study separates the dynamic and thermodynamic contributions from SIC intensification anomalies and indicates that different combinations of ENSO and SAM can have different impacts in driving regional Antarctic sea ice changes through atmospheric and oceanic processes. However, the accurate contributions of mechanical redistributions still cannot be estimated from observations, which might be underestimated in this study. Moreover, the surface, bottom, and lateral freezing and melting processes are still mixed together. A detailed decomposition method using observations and models should be researched in the future in order to investigate the accurate proportions of each contributing term.

Acknowledgments. The authors wish to thank three anonymous reviewers for their very helpful comments and suggestions. This is a contribution to the Year of Polar Prediction (YOPP), a flagship activity of the Polar Prediction Project (PPP), initiated by the World Weather Research Programme (WWRP) of the World Meteorological Organization (WMO). We acknowledge the WMO WWRP for its role in coordinating this International Research activity. This study is supported by the National Natural Science Foundation of China (41941009, 42006191, 41922044), the National Key Research and Development Program of China (2022YFE0106300), the Guangdong Basic and Applied Basic Research Foundation (2020B1515020025), and the Norges Forskningsråd (Grant 328886).

Data availability statement. NSIDC sea ice concentration data are available at <https://nsidc.org/data/nsidc-0051/versions/2> and sea ice motion data are available at <https://nsidc.org/data/nsidc-0116/versions/4>. ERA5 reanalysis data are available at <https://www.ecmwf.int/en/forecasts/datasets/reanalysis-datasets/era5>. The AAO index and ONI are accessible at <https://www.cpc.ncep.noaa.gov>.

REFERENCES

- Arrigo, K. R., 2014: Sea ice ecosystems. *Annu. Rev. Mar. Sci.*, **6**, 439–467, <https://doi.org/10.1146/annurev-marine-010213-135103>.
- Ayres, H. C., and J. A. Screen, 2019: Multimodel analysis of the atmospheric response to Antarctic sea ice loss at quadrupled CO₂. *Geophys. Res. Lett.*, **46**, 9861–9869, <https://doi.org/10.1029/2019GL083653>.
- Campitelli, E., L. B. Díaz, and C. Vera, 2022: Assessment of zonally symmetric and asymmetric components of the Southern Annular Mode using a novel approach. *Climate Dyn.*, **58**, 161–178, <https://doi.org/10.1007/s00382-021-05896-5>.
- Cavalieri, D. J., C. L. Parkinson, P. Gloersen, and H. J. Zwally, 1996: Sea ice concentrations from Nimbus-7 SMMR and DMSP SSM/I-SSMIS passive microwave data, Version 1

- (NSIDC-0051). Updated yearly, NASA National Snow and Ice Data Center Distributed Active Archive Center, <https://doi.org/10.5067/8GQ8LZQVL0VL>.
- Cerovečki, I., R. Sun, D. H. Bromwich, X. Zou, M. R. Mazloff, and S.-H. Wang, 2022: Impact of downward longwave radiative deficits on Antarctic sea-ice extent predictability during the sea ice growth period. *Environ. Res. Lett.*, **17**, 084008, <https://doi.org/10.1088/1748-9326/ac7d66>.
- Ciasto, L. M., and M. H. England, 2011: Observed ENSO teleconnections to Southern Ocean SST anomalies diagnosed from a surface mixed layer heat budget. *Geophys. Res. Lett.*, **38**, L09701, <https://doi.org/10.1029/2011GL046895>.
- Crosby, D. S., L. C. Breaker, and W. H. Gemmill, 1993: A proposed definition for vector correlation in geophysics: Theory and application. *J. Atmos. Oceanic Technol.*, **10**, 355–367, [https://doi.org/10.1175/1520-0426\(1993\)010<0355:APDFVC>2.0.CO;2](https://doi.org/10.1175/1520-0426(1993)010<0355:APDFVC>2.0.CO;2).
- Ding, Q., E. J. Steig, D. S. Battisti, and J. M. Wallace, 2012: Influence of the tropics on the Southern Annular Mode. *J. Climate*, **25**, 6330–6348, <https://doi.org/10.1175/JCLI-D-11-00523.1>.
- Doddridge, E. W., and J. Marshall, 2017: Modulation of the seasonal cycle of Antarctic sea ice extent related to the Southern Annular Mode. *Geophys. Res. Lett.*, **44**, 9761–9768, <https://doi.org/10.1002/2017GL074319>.
- Dong, X., Y. Wang, S. Hou, M. Ding, B. Yin, and Y. Zhang, 2020: Robustness of the recent global atmospheric reanalyses for Antarctic near-surface wind speed climatology. *J. Climate*, **33**, 4027–4043, <https://doi.org/10.1175/JCLI-D-19-0648.1>.
- Eicken, H., 1992: The role of sea ice in structuring Antarctic ecosystems. *Polar Biol.*, **12**, 3–13, <https://doi.org/10.1007/BF00239960>.
- Ferrari, R., M. F. Jansen, J. F. Adkins, A. Burke, A. L. Stewart, and A. F. Thompson, 2014: Antarctic sea ice control on ocean circulation in present and glacial climates. *Proc. Natl. Acad. Sci. USA*, **111**, 8753–8758, <https://doi.org/10.1073/pnas.1323922111>.
- Ferreira, D., J. Marshall, C. M. Bitz, S. Solomon, and A. Plumb, 2015: Antarctic Ocean and sea ice response to ozone depletion: A two-time-scale problem. *J. Climate*, **28**, 1206–1226, <https://doi.org/10.1175/JCLI-D-14-00313.1>.
- Fogt, R. L., and G. J. Marshall, 2020: The Southern Annular Mode: Variability, trends, and climate impacts across the Southern Hemisphere. *Wiley Interdiscip. Rev.: Climate Change*, **11**, e652, <https://doi.org/10.1002/wcc.652>.
- , D. H. Bromwich, and K. M. Hines, 2011: Understanding the SAM influence on the South Pacific ENSO teleconnection. *Climate Dyn.*, **36**, 1555–1576, <https://doi.org/10.1007/s00382-010-0905-0>.
- , J. M. Jones, and J. Renwick, 2012: Seasonal zonal asymmetries in the Southern Annular Mode and their impact on regional temperature anomalies. *J. Climate*, **25**, 6253–6270, <https://doi.org/10.1175/JCLI-D-11-00474.1>.
- Gong, D., and S. Wang, 1999: Definition of Antarctic Oscillation index. *Geophys. Res. Lett.*, **26**, 459–462, <https://doi.org/10.1029/1999GL900003>.
- Gong, T., S. B. Feldstein, and D. Luo, 2010: The impact of ENSO on wave breaking and Southern Annular Mode events. *J. Atmos. Sci.*, **67**, 2854–2870, <https://doi.org/10.1175/2010JAS3311.1>.
- Hagman, D., 2022: Unraveling the uncertainties of bulk-derived heat fluxes: A case study for the Southern Ocean. *EGU General Assembly 2022*, Vienna, Austria, EGU22-393, <https://doi.org/10.5194/egusphere-egu22-393>.
- Hersbach, H., and Coauthors, 2020: The ERA5 global reanalysis. *Quart. J. Roy. Meteor. Soc.*, **146**, 1999–2049, <https://doi.org/10.1002/qj.3803>.
- Hobbs, W. R., R. Massom, S. Stammerjohn, P. Reid, G. Williams, and W. Meier, 2016: A review of recent changes in Southern Ocean sea ice, their drivers and forcings. *Global Planet. Change*, **143**, 228–250, <https://doi.org/10.1016/j.gloplacha.2016.06.008>.
- Holland, P. R., and R. Kwok, 2012: Wind-driven trends in Antarctic sea-ice drift. *Nat. Geosci.*, **5**, 872–875, <https://doi.org/10.1038/ngeo1627>.
- , and N. Kimura, 2016: Observed concentration budgets of Arctic and Antarctic sea ice. *J. Climate*, **29**, 5241–5249, <https://doi.org/10.1175/JCLI-D-16-0121.1>.
- Holmes, C. R., P. R. Holland, and T. J. Bracegirdle, 2019: Compensating biases and a noteworthy success in the CMIP5 representation of Antarctic sea ice processes. *Geophys. Res. Lett.*, **46**, 4299–4307, <https://doi.org/10.1029/2018GL081796>.
- Hoskins, B. J., and D. J. Karoly, 1981: The steady linear response of a spherical atmosphere to thermal and orographic forcing. *J. Atmos. Sci.*, **38**, 1179–1196, [https://doi.org/10.1175/1520-0469\(1981\)038<1179:TSLROA>2.0.CO;2](https://doi.org/10.1175/1520-0469(1981)038<1179:TSLROA>2.0.CO;2).
- Huang, B., and Coauthors, 2017: Extended Reconstructed Sea Surface Temperature, version 5 (ERSSTv5): Upgrades, validations, and intercomparisons. *J. Climate*, **30**, 8179–8205, <https://doi.org/10.1175/JCLI-D-16-0836.1>.
- Jin, D., and B. P. Kirtman, 2009: Why the Southern Hemisphere ENSO responses lead ENSO. *J. Geophys. Res.*, **114**, D23101, <https://doi.org/10.1029/2009JD012657>.
- Karoly, D. J., 1989: Southern Hemisphere circulation features associated with El Niño–Southern Oscillation events. *J. Climate*, **2**, 1239–1252, [https://doi.org/10.1175/1520-0442\(1989\)002<1239:SHCFAW>2.0.CO;2](https://doi.org/10.1175/1520-0442(1989)002<1239:SHCFAW>2.0.CO;2).
- King, J. C., G. J. Marshall, S. Colwell, S. Arndt, C. Allen-Sader, and T. Phillips, 2022: The performance of the ERA-Interim and ERA5 atmospheric reanalyses over Weddell Sea pack ice. *J. Geophys. Res. Oceans*, **127**, e2022JC018805, <https://doi.org/10.1029/2022JC018805>.
- Kirkman, C. H., and C. M. Bitz, 2011: The effect of the sea ice freshwater flux on Southern Ocean temperatures in CCSM3: Deep-ocean warming and delayed surface warming. *J. Climate*, **24**, 2224–2237, <https://doi.org/10.1175/2010JCLI3625.1>.
- Kurtz, N. T., T. Markus, S. L. Farrell, D. L. Worthen, and L. N. Boisvert, 2011: Observations of recent Arctic sea ice volume loss and its impact on ocean-atmosphere energy exchange and ice production. *J. Geophys. Res.*, **116**, C04015, <https://doi.org/10.1029/2010JC006235>.
- Kwok, R., and J. C. Comiso, 2002: Southern Ocean climate and sea ice anomalies associated with the Southern Oscillation. *J. Climate*, **15**, 487–501, [https://doi.org/10.1175/1520-0442\(2002\)015<0487:SOCASI>2.0.CO;2](https://doi.org/10.1175/1520-0442(2002)015<0487:SOCASI>2.0.CO;2).
- , —, T. Lee, and P. R. Holland, 2016: Linked trends in the South Pacific sea ice edge and Southern Oscillation index. *Geophys. Res. Lett.*, **43**, 10295–10302, <https://doi.org/10.1002/2016GL070655>.
- Lecomte, O., H. Goosse, T. Fichefet, P. R. Holland, P. Uotila, V. Zunz, and N. Kimura, 2016: Impact of surface wind biases on the Antarctic sea ice concentration budget in climate models. *Ocean Modell.*, **105**, 60–70, <https://doi.org/10.1016/j.ocemod.2016.08.001>.
- L’Heureux, M. L., and D. W. J. Thompson, 2006: Observed relationships between the El Niño–Southern Oscillation and the

- extratropical zonal-mean circulation. *J. Climate*, **19**, 276–287, <https://doi.org/10.1175/JCLI3617.1>.
- Liu, J., J. A. Curry, and D. G. Martinson, 2004: Interpretation of recent Antarctic sea ice variability. *Geophys. Res. Lett.*, **31**, L02205, <https://doi.org/10.1029/2003GL018732>.
- Maksym, T., 2019: Arctic and Antarctic sea ice change: Contrasts, commonalities, and causes. *Annu. Rev. Mar. Sci.*, **11**, 187–213, <https://doi.org/10.1146/annurev-marine-010816-060610>.
- Mo, K. C., and R. W. Higgins, 1998: The Pacific–South American modes and tropical convection during the Southern Hemisphere winter. *Mon. Wea. Rev.*, **126**, 1581–1596, [https://doi.org/10.1175/1520-0493\(1998\)126<1581:TPSAMA>2.0.CO;2](https://doi.org/10.1175/1520-0493(1998)126<1581:TPSAMA>2.0.CO;2).
- Notz, D., and J. Stroeve, 2016: Observed Arctic sea-ice loss directly follows anthropogenic CO₂ emission. *Science*, **354**, 747–750, <https://doi.org/10.1126/science.aag2345>.
- Parkinson, C. L., 2019: A 40-y record reveals gradual Antarctic sea ice increases followed by decreases at rates far exceeding the rates seen in the Arctic. *Proc. Natl. Acad. Sci. USA*, **116**, 14 414–14 423, <https://doi.org/10.1073/pnas.1906556116>.
- Pettitt, A. N., 2014: Mann–Whitney–Wilcoxon statistic. *Wiley StatsRef: Statistics Reference Online*, N. Balakrishnan et al., Eds., Wiley, <https://doi.org/10.1002/9781118445112.stat02754>.
- Pezza, A. B., H. A. Rashid, and I. Simmonds, 2012: Climate links and recent extremes in Antarctic sea ice, high-latitude cyclones, Southern Annular Mode and ENSO. *Climate Dyn.*, **38**, 57–73, <https://doi.org/10.1007/s00382-011-1044-y>.
- Polvani, L. M., and Coauthors, 2021: Interannual SAM modulation of Antarctic sea ice extent does not account for its long-term trends, pointing to a limited role for ozone depletion. *Geophys. Res. Lett.*, **48**, e2021GL094871, <https://doi.org/10.1029/2021GL094871>.
- Pope, J. O., P. R. Holland, A. Orr, G. J. Marshall, and T. Phillips, 2017: The impacts of El Niño on the observed sea ice budget of West Antarctica. *Geophys. Res. Lett.*, **44**, 6200–6208, <https://doi.org/10.1002/2017GL073414>.
- Raphael, M. N., 2003: Impact of observed sea-ice concentration on the Southern Hemisphere extratropical atmospheric circulation in summer. *J. Geophys. Res.*, **108**, 4687, <https://doi.org/10.1029/2002JD003308>.
- Roach, L. A., and Coauthors, 2020: Antarctic sea ice area in CMIP6. *Geophys. Res. Lett.*, **47**, e2019GL086729, <https://doi.org/10.1029/2019GL086729>.
- Rogers, J. C., and H. van Loon, 1982: Spatial variability of sea level pressure and 500 mb height anomalies over the Southern Hemisphere. *Mon. Wea. Rev.*, **110**, 1375–1392, [https://doi.org/10.1175/1520-0493\(1982\)110<1375:SVOSLP>2.0.CO;2](https://doi.org/10.1175/1520-0493(1982)110<1375:SVOSLP>2.0.CO;2).
- Seager, R., N. Harnik, Y. Kushnir, W. Robinson, and J. Miller, 2003: Mechanisms of hemispherically symmetric climate variability. *J. Climate*, **16**, 2960–2978, [https://doi.org/10.1175/1520-0442\(2003\)016<2960:MOHSCV>2.0.CO;2](https://doi.org/10.1175/1520-0442(2003)016<2960:MOHSCV>2.0.CO;2).
- Sen Gupta, A., and M. H. England, 2006: Coupled ocean–atmosphere–ice response to variations in the Southern Annular Mode. *J. Climate*, **19**, 4457–4486, <https://doi.org/10.1175/JCLI3843.1>.
- Serreze, M. C., and W. N. Meier, 2019: The Arctic’s sea ice cover: Trends, variability, predictability, and comparisons to the Antarctic. *Ann. N. Y. Acad. Sci.*, **1436**, 36–53, <https://doi.org/10.1111/nyas.13856>.
- Shu, Q., Z. Song, and F. Qiao, 2015: Assessment of sea ice simulations in the CMIP5 models. *Cryosphere*, **9**, 399–409, <https://doi.org/10.5194/tc-9-399-2015>.
- Simpkins, G. R., L. M. Ciasto, D. W. J. Thompson, and M. H. England, 2012: Seasonal relationships between large-scale climate variability and Antarctic sea ice concentration. *J. Climate*, **25**, 5451–5469, <https://doi.org/10.1175/JCLI-D-11-00367.1>.
- Smith, D. M., N. J. Dunstone, A. A. Scaife, E. K. Fiedler, D. Copsey, and S. C. Hardiman, 2017: Atmospheric response to Arctic and Antarctic sea ice: The importance of ocean–atmosphere coupling and the background state. *J. Climate*, **30**, 4547–4565, <https://doi.org/10.1175/JCLI-D-16-0564.1>.
- Song, H.-J., E. Choi, G.-H. Lim, Y. H. Kim, J.-S. Kug, and S.-W. Yeh, 2011: The central Pacific as the export region of the El Niño–Southern Oscillation sea surface temperature anomaly to Antarctic sea ice: The importance of ocean–atmosphere coupling and the background state. *J. Geophys. Res.*, **116**, D21113, <https://doi.org/10.1029/2011JD015645>.
- Søren, R., and Coauthors, 2011: Sea ice contribution to the air–sea CO₂ exchange in the Arctic and Southern Oceans. *Tellus*, **63B**, 823–830, <https://doi.org/10.1111/j.1600-0889.2011.00571.x>.
- Stammerjohn, S. E., D. G. Martinson, R. C. Smith, X. Yuan, and D. Rind, 2008: Trends in Antarctic annual sea ice retreat and advance and their relation to El Niño–Southern Oscillation and Southern Annular Mode variability. *J. Geophys. Res.*, **113**, C03S90, <https://doi.org/10.1029/2007JC004269>.
- Stroeve, J., M. M. Holland, W. Meier, T. Scambos, and M. Serreze, 2007: Arctic sea ice decline: Faster than forecast. *Geophys. Res. Lett.*, **34**, L09501, <https://doi.org/10.1029/2007GL029703>.
- Stuart, A., K. Ord, and S. Arnold, 2009: Partial and multiple correlation. *Kendall’s Advanced Theory of Statistics*, A. Stuart, K. Ord, and S. Arnold, Eds., Vol. 2A, *Classical Inference and the Linear Model*, 6th ed. Wiley, 510–537.
- Takaya, K., and H. Nakamura, 2001: A formulation of a phase-independent wave-activity flux for stationary and migratory quasigeostrophic eddies on a zonally varying basic flow. *J. Atmos. Sci.*, **58**, 608–627, [https://doi.org/10.1175/1520-0469\(2001\)058<0608:AFOAPI>2.0.CO;2](https://doi.org/10.1175/1520-0469(2001)058<0608:AFOAPI>2.0.CO;2).
- Tetner, D., E. Thomas, and C. Allen, 2019: A validation of ERA5 reanalysis data in the southern Antarctic Peninsula–Ellsworth land region, and its implications for ice core studies. *Geosciences*, **9**, 289, <https://doi.org/10.3390/geosciences9070289>.
- Thompson, D. W. J., and J. M. Wallace, 2000: Annular modes in the extratropical circulation. Part I: Month-to-month variability. *J. Climate*, **13**, 1000–1016, [https://doi.org/10.1175/1520-0442\(2000\)013<1000:AMITEC>2.0.CO;2](https://doi.org/10.1175/1520-0442(2000)013<1000:AMITEC>2.0.CO;2).
- , and S. Solomon, 2002: Interpretation of recent Southern Hemisphere climate change. *Science*, **296**, 895–899, <https://doi.org/10.1126/science.1069270>.
- Trenberth, K. E., 1986: An assessment of the impact of transient eddies on the zonal flow during a blocking episode using localized Eliassen–Palm flux diagnostics. *J. Atmos. Sci.*, **43**, 2070–2087, [https://doi.org/10.1175/1520-0469\(1986\)043<2070:AAOTIO>2.0.CO;2](https://doi.org/10.1175/1520-0469(1986)043<2070:AAOTIO>2.0.CO;2).
- , 1991: Storm tracks in the Southern Hemisphere. *J. Atmos. Sci.*, **48**, 2159–2178, [https://doi.org/10.1175/1520-0469\(1991\)048<2159:STITSH>2.0.CO;2](https://doi.org/10.1175/1520-0469(1991)048<2159:STITSH>2.0.CO;2).
- Tschudi, M., W. N. Meier, J. S. Stewart, C. Fowler, and J. Maslanik, 2019: Polar Pathfinder Daily 25 km EASE-Grid Sea Ice Motion Vectors, version 4 (NSIDC-0116). NSIDC, accessed 3 April 2022, <https://doi.org/10.5067/INAWUWO7QH7B>.
- Turner, J., 2004: The El Niño–Southern Oscillation and Antarctica. *Int. J. Climatol.*, **24** (1), 1–31, <https://doi.org/10.1002/joc.965>.
- , and J. Comiso, 2017: Solve Antarctica’s sea-ice puzzle. *Nature*, **547**, 275–277, <https://doi.org/10.1038/547275a>.
- , and Coauthors, 2022: Record low Antarctic sea ice cover in February 2022. *Geophys. Res. Lett.*, **49**, e2022GL098904, <https://doi.org/10.1029/2022GL098904>.

- Uotila, P., P. R. Holland, T. Vihma, S. J. Marsland, and N. Kimura, 2014: Is realistic Antarctic sea-ice extent in climate models the result of excessive ice drift? *Ocean Modell.*, **79**, 33–42, <https://doi.org/10.1016/j.ocemod.2014.04.004>.
- Vihma, T., 2014: Effects of Arctic sea ice decline on weather and climate: A review. *Surv. Geophys.*, **35**, 1175–1214, <https://doi.org/10.1007/s10712-014-9284-0>.
- Wang, H., A. R. Klekociuk, W. J. R. French, S. P. Alexander, and T. A. Warner, 2020: Measurements of cloud radiative effect across the Southern Ocean (43°S–79°S, 63°E–158°W). *Atmosphere*, **11**, 949, <https://doi.org/10.3390/atmos11090949>.
- Wang, J., H. Luo, Q. Yang, J. Liu, L. Yu, Q. Shi, and B. Han, 2022: An unprecedented record low Antarctic sea-ice extent during austral summer 2022. *Adv. Atmos. Sci.*, **39**, 1591–1597, <https://doi.org/10.1007/s00376-022-2087-1>.
- Wang, Y., K. Hu, G. Huang, and W. Tao, 2021: Asymmetric impacts of El Niño and La Niña on the Pacific–North American teleconnection pattern: The role of subtropical jet stream. *Environ. Res. Lett.*, **16**, 114040, <https://doi.org/10.1088/1748-9326/ac31ed>.
- , G. Huang, K. Hu, W. Tao, X. Li, H. Gong, L. Gu, and W. Zhang, 2022: Asymmetric impacts of El Niño and La Niña on the Pacific–South America teleconnection pattern. *J. Climate*, **35**, 1825–1838, <https://doi.org/10.1175/JCLI-D-21-0285.1>.
- Welhouse, L. J., M. A. Lazzara, L. M. Keller, G. J. Tripoli, and M. H. Hitchman, 2016: Composite analysis of the effects of ENSO events on Antarctica. *J. Climate*, **29**, 1797–1808, <https://doi.org/10.1175/JCLI-D-15-0108.1>.
- Wilson, A. B., D. H. Bromwich, and K. M. Hines, 2016: Simulating the mutual forcing of anomalous high southern latitude atmospheric circulation by El Niño flavors and the Southern Annular Mode. *J. Climate*, **29**, 2291–2309, <https://doi.org/10.1175/JCLI-D-15-0361.1>.
- Wilson, E. A., S. C. Riser, E. C. Campbell, and A. P. S. Wong, 2019: Winter upper-ocean stability and ice–ocean feedbacks in the sea ice–covered Southern Ocean. *J. Phys. Oceanogr.*, **49**, 1099–1117, <https://doi.org/10.1175/JPO-D-18-0184.1>.
- Yadav, J., A. Kumar, A. Srivastava, and R. Mohan, 2022: Sea ice variability and trends in the Indian Ocean sector of Antarctica: Interaction with ENSO and SAM. *Environ. Res.*, **212**, 113481, <https://doi.org/10.1016/j.envres.2022.113481>.
- Yeo, S.-R., and K.-Y. Kim, 2015: Decadal changes in the Southern Hemisphere sea surface temperature in association with El Niño–Southern Oscillation and Southern Annular Mode. *Climate Dyn.*, **45**, 3227–3242, <https://doi.org/10.1007/s00382-015-2535-z>.
- Yiu, Y. Y. S., and A. C. Maycock, 2019: On the seasonality of the El Niño teleconnection to the Amundsen Sea region. *J. Climate*, **32**, 4829–4845, <https://doi.org/10.1175/JCLI-D-18-0813.1>.
- Yu, J.-Y., H. Paek, E. S. Saltzman, and T. Lee, 2015: The early 1990s change in ENSO–PSA–SAM relationships and its impact on Southern Hemisphere climate. *J. Climate*, **28**, 9393–9408, <https://doi.org/10.1175/JCLI-D-15-0335.1>.
- Yu, L., and Coauthors, 2011: Interpretation of recent trends in Antarctic sea ice concentration. *J. Appl. Remote Sens.*, **5**, 053557, <https://doi.org/10.1117/1.3643691>.
- Yuan, N., M. Ding, J. Ludescher, and A. Bunde, 2017: Increase of the Antarctic sea ice extent is highly significant only in the Ross Sea. *Sci. Rep.*, **7**, 41096, <https://doi.org/10.1038/srep41096>.
- Yuan, X., 2004: ENSO-related impacts on Antarctic sea ice: A synthesis of phenomenon and mechanisms. *Antarct. Sci.*, **16**, 415–425, <https://doi.org/10.1017/S0954102004002238>.
- , and D. G. Martinson, 2001: The Antarctic dipole and its predictability. *Geophys. Res. Lett.*, **28**, 3609–3612, <https://doi.org/10.1029/2001GL012969>.
- , M. R. Kaplan, and M. A. Cane, 2018: The interconnected global climate system—A review of tropical–polar teleconnections. *J. Climate*, **31**, 5765–5792, <https://doi.org/10.1175/JCLI-D-16-0637.1>.
- Zhang, C., T. Li, and S. Li, 2021: Impacts of CP and EP El Niño events on the Antarctic sea ice in austral spring. *J. Climate*, **34**, 9327–9348, <https://doi.org/10.1175/JCLI-D-21-0002.1>.
- Zhu, J., A. Xie, X. Qin, Y. Wang, B. Xu, and Y. Wang, 2021: An assessment of ERA5 reanalysis for Antarctic near-surface air temperature. *Atmosphere*, **12**, 217, <https://doi.org/10.3390/atmos12020217>.
- Zubiaurre, I., and N. Calvo, 2012: The El Niño–Southern Oscillation (ENSO) Modoki signal in the stratosphere. *J. Geophys. Res.*, **117**, D04104, <https://doi.org/10.1029/2011JD016690>.